Mem. S.A.It. Vol. 93, 245

Memorie della

Science case study and scientific simulations for the enhanced X-ray Timing Polarimetry mission, eXTP

A. De Rosa[1], G. F. Burgio[2], T. Di Salvo[3], A. Drago[4], R. La Placa[5,6], R. Serafinelli[1], A. Gambino[3], L. Gualtieri[5], A. Maselli[7,8], M. Feroci[1], L. Stella[9], I. Bombaci[10], L. Burderi[11], R. Campana[12], F. Capitanio[1], P. Casella[9], A. D'Aì[13], F. D'Ammando[14], D. De Martino[15], Y. Evangelista[1], V. Ferrari[5], E. Nardini[16], M. Orlandini[12], L. Pacciani[1], G. Pagliara[4], P. Pani[5], A. Riggio[11], G. Rodriguez[13] A. Sanna[11], H.J. Schulze[2], R. Taverna[17], F. Tombesi[6], S. Vercellone[18]

[1] INAF - Istituto di Astrofisica e Planetologia Spaziali (IAPS), via Fosso del Cavaliere, Roma, I-00133, Italy, e-mail: alessandra.derosa@inaf.it
[2] INFN Sezione di Catania, Via S. Sofia 64, I-95123 Catania, Italy
[3] Dipartimento di Fisica e Chimica, Università di Palermo, via Archirafi 36, 90123, Palermo, Italy
[4] Dipartimento di Fisica e Scienze della Terra, Università di Ferrara, Via Saragat 1, I-44122 Ferrara, Italy
[5] Dipartimento di Fisica, "Sapienza" Università di Roma, Piazzale Aldo Moro 5, I-00185, Roma, Italy
[6] Department of Physics, University of Rome "Tor Vergata", Via della Ricerca Scientifica 1, I-00133 Rome, Italy
[7] Gran Sasso Science Institute (GSSI), I-67100 L'Aquila, Italy
[8] INFN, Laboratori Nazionali del Gran Sasso, I-67100 Assergi, Italy
[9] INAF - Osservatorio Astronomico di Roma, via Frascati 33, 00040 Monte Porzio Catone, Roma, Italy
[10] Dipartimento di Fisica "Enrico Fermi", Università di Pisa, Largo B. Pontecorvo 3, I-56127 Pisa, Italy
The remaining affiliations can be found at the end of the paper.

Received: 17 December 2021; Accepted:30 May 2022

Abstract. The X-ray astronomy mission eXTP (enhanced X-ray Timing Polarimetry) is designed to study matter under extreme conditions of density, gravity and magnetism. Primary goals are the determination of the equation of state (EoS) of matter at supranuclear density, the physics in extremely strong magnetic fields, the study of accretion in strong-field gravity (SFG) regime. Primary targets include isolated and binary neutron stars, strong magnetic-field systems like magnetars, and stellar-mass and supermassive black holes. In this paper we report about key observations and simulations with eXTP on the primary objectives involving accretion under SFG regimes and determination of NS-EoS.

Key words. X-rays – Black Holes – Neutron stars – accretion – dense matter – Astronomical instrumentation, methods and techniques

1. Introduction

Astrophysical sources such as Neutron Stars (NSs) and Black Holes (BHs), are ideal laboratories to understand the state of matter and fundamental interactions such as gravity and strong force by studying the plasmas under extreme conditions that cannot be attained on Earth. Densities in the cores of NSs can reach 10 times the density of atomic nuclei, forming states of matter that cannot be produced in laboratories. X-ray emitting matter which accretes close to the event horizon of BHs (supermassive in Active Galactic Nuclei, AGN, and stellar-mass BHs in X-ray Binaries, XRBs) or close to the surface of NSs offers powerful diagnostics to study the very deep potential-well generated by the central object, infer its mass and spin, and verify crucial predictions of General Relativity in the strong field regime (SFG). These questions are the primary goals of the eXTP mission (De Rosa et al. 2019; Watts et al. 2019; Santangelo et al. 2019; in't Zand et al. 2019). The scientific payload of eXTP is discussed in detail in Zhang et al. (2019). It consists of the spectroscopic focusing array (SFA), the polarimetry focusing array (PFA), the large area detector (LAD) and the wide field monitor (WFM). The combination of the SFA (an array of nine identical X-ray mirror and silicon drift detector combinations, covering the 0.5–10 keV and with 180 eV resolution at 6 keV) and the LAD (a set of large-area collimated silicon drift detectors in the 2–50 keV energy range and with 260 eV resolution at 6 keV) provides eXTP's large-area and fast-timing and spectroscopy capability. The total LAD+SFA effective area is 4 m^2 at 6 keV and the silicon drift detectors will allow one to sample extremely high count rates at high time resolution (10 μs) with minimal deadtime. The PFA will provide another independent X-ray diagnostic, it consists of four identical X-ray telescopes sensitive at 2–10 keV, with angular resolution better than 30 arcsec and a total effective area of about 500 m^2 at 3 keV (including the detector efficiency). The monitoring needed for the primary eXTP scientific objectives is guaranteed thanks to the WFM, consisting of 6 coded-mask cameras covering 3.7 sr of the sky with 4 mCrab sensitivity at 2–50 keV for an exposure time of 1 day and 0.2 mCrab combining 1 yr of observations outside the galactic plane. We present in this paper the study and detailed simulations of different scientific diagnostics involving accretion around BHs (in AGN and XRB, Sect. 2) and NS equation of state (Sect. 3). Our contribution as support to the mission is described in Sect. 4

2. Accreting compact objects: Mapping the inner regions

Super-massive BHs (SMBHs) in AGN and stellar-mass BHs in XRBs, provide a powerful laboratory to study the accretion flows of matter under the SFG regime. An optically thick accretion disk extending down to the innermost stable circular orbit (ISCO) is formed and the bulk of emission is produced within a few gravitational radii ($R_g = GM/c^2$) from the compact object. When the disk is externally illuminated, e.g., by the hot Comptonizing gas (often referred to as the "corona") which is responsible for the power-law X-ray emission component of AGN and XRBs, an iron emission line is produced together with a reflection continuum. The latter manifests itself as a broad bump starting at a few keV and peaking around 30 keV. The reflection is due to direct Compton scattering, with low-energy absorption due to photoelectric interaction with the most abundant atomic species, and the corresponding fluorescence features are produced. The combination of special relativistic (Doppler effect and relativistic aberration) and GR (gravitational redshift, light bending) effects contribute to broaden and distort the intrinsically narrow Fe K line. X-ray measurements of accretion under the SFG regime can then be used to infer the two most fundamental BH parameters: mass and spin (e.g., Fabian et al. 1989). In the following, we report on the powerful spectral timing polarimetry techniques provided by eXTP for probing matter flows in the SFG regime.

2.1. High-order Images

The broad, asymmetrical Fe K lines encapsulate information on the size of the disk, incli-

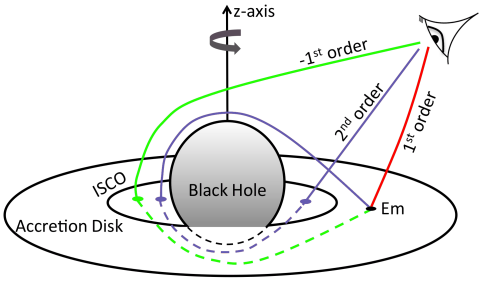

Fig. 1. Sketch of three photon geodesics starting from a point $E_{\rm m}$ on a BH accretion disk. The first order trajectory (red) produces the direct image. The minus-first order photons (green) originate from below the disk, passing between the BH and the ISCO, and thus generating the first indirect image. Finally, the trajectory looping around the BH (purple) gives rise to the second order direct image. Adapted from Falanga et al. (2021).

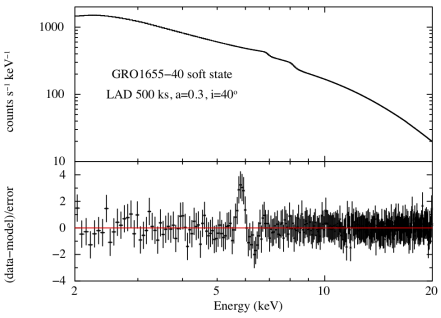

Fig. 2. GRO J1655-40 in a low state: the 500 ks simulated eXTP/LAD spectrum is presented in the upper panel, while the lower panel shows the residuals with respect to a model not including the HOIs component. Adapted from (Falanga et al. 2021).

nation, ionisation and source of illumination, and have been observed from both XRBs and AGNs. While in general models of the disk emission only account for the first direct image of the disk, an infinite number of photon trajectories start from it, including higher-order images (HOIs) produced by strongly deflected rays from the disk which cross the plunging region, located between the ISCO radius and the event horizon of a Kerr BH (see Fig. 1). In particular, the plunging region in systems accreting at $\lesssim$ 1% the Eddington rate would be optically thin for the most part, allowing photons on such trajectories to reach the observer (Falanga et al. 2021). HOIs are usually neglected since the overall contribution to the flux is quite limited: in the case of Fe Kα, typical values range from 0.1% to 1.5% of the total flux in the profiles. However, the specific flux ratio at some energies can reach 5 – 7%, depending on system parameters, attaining higher values for BHs with low and negative spin ($a \lesssim 0.3$) and disks with intermediate inclination angle ($i \sim 40°$). Simulated eXTP-LAD observations of 21 different configurations that took into account HOIs in the Fe Kα profile were produced and later analysed with one current Fe Kα model, `relline` (Dauser et al. 2010), within XSPEC. Being no model publicly available for data fitting accounting for HOIs from the disk, we focused our study on the effects of this absence on the parameter values retrieved during X-ray spectral analysis. Thanks to the unprecedented effective area of the LAD, the spectral signature of the HOIs can emerge from the background, although in most cases it is then leveled out during fitting by changes in the other parameters (see Fig. 2 for one of the few examples in which the residuals are still visible after the analysis). This however leads primarily to a systematic overestimate of the best-fit spin, which is rendered incompatible with its input value in more than half the simulations run, even considering rather large 95%-confidence intervals (Falanga et al. 2021). The bias is strongest in configurations with $i = 60°$, which display incompatible best-fit spins in more than 80% of the cases, with overestimates often reaching $a_{fit} - a_{input} \sim 0.3$. This analysis demonstrate that HOIs should be taken into account in modelling LAD data, and its confirmation by eXTP observations would provide a test of one of the finest effects of GR in SFG.

2.2. X-ray polarimetry in stellar-mass BH accretion disks

GR can influence the polarization properties of the emission from the accretion disk of stellar-

mass BHs. Photon polarization vectors are rotated during their parallel transport along null geodesics (Stark & Connors 1977; Connors & Stark 1977), modifying the polarization degree observed at infinity with respect to the polarization pattern at the disk. Returning photons (i.e. photons forced by SFG to return to the disk before being eventually reflected towards the observer) can deeply modify both the spectral and polarization properties of the radiation collected at infinity (Schnittman & Krolik 2009; Taverna et al. 2020). In particular, returning radiation is expected to dominate at high energies, since photons emitted closer to the BH (at higher temperature of the disk) are more likely bent back to the disk, while direct radiation is prevalent at low energies. When large optical depths for the disk are considered, direct and returning components are polarized orthogonally, i.e. with photon polarization vectors perpendicular and parallel to the disk axis projection in the plane of the sky, respectively. As a consequence, the polarization degree and angle are expected to strongly depend on the photon energy, with the polarization angle swinging by 90° and the polarization degree attaining a minimum when the reflected component starts to dominate in the spectrum. Numerical simulations (Schnittman & Krolik 2009; Taverna et al. 2020) show that the energy at which the polarization angle swings and the minimum in the polarization degree change for different values of the BH mass and spin. A simultaneous spectral and polarization measurement of this kind of sources is within the reach of IXPE (Weisskopf et al. 2016) and, with higher signal-to-noise ratio, of eXTP. These data can hence provide further, independent constraints for estimating these two important BH parameters. In fact SFA+LAD will allow the measurement of BH spin with 3–4% accuracy through only a 100-s exposure of a 0.1 Crab source (De Rosa et al. 2019), while longer PFA observations, of the order of 100 ks, will allow us to reach a 0.4% minimum polarization degree (MDP) putting independent constraints on BH spin measurements. Moreover, absorption effects on the disk tend to increase the intrinsic polarization degree of the emitted radiation (up to values larger than

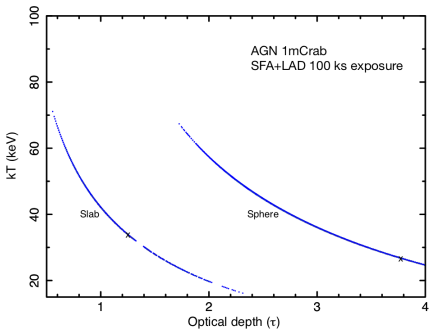

Fig. 3. Contour plot at 3σ (99.7%) confidence level between the coronal temperature kT and the optical depth τ. The two cases of slab and spherical corona are shown together for a simulated 100 ks SFA+LAD spectrum of an AGN with a flux of $\sim$ 1 mCrab in the 2 – 10 keV band.

~20%) compared to the predicted value in the pure-scattering limit (less than ~10%, Taverna et al. 2021, and references therein), which goes in the direction of making more feasible in terms of exposure a polarization measurement for these sources.

2.3. AGN Hot coronae

The X-ray emission of AGN is thought to be produced by thermal Comptonization of UV radiation emitted by the accretion disk (e.g., Haardt & Maraschi 1991). This process occurs in a small ($\sim 10R_g$) region located in the innermost part of the AGN, made up of very hot ($T \sim 10^9$ K) electron plasma, the so-called corona. The shape of the coronal X-ray spectrum is well approximated by a power law up to a cut-off energy E_c, where the power law breaks. The cut-off energy and the spectral slope are related to the physical properties of the corona, i.e. the coronal temperature kT_e and the optical depth τ (e.g Petrucci et al. 2001). However, the relation between physical and observed parameters strongly depend on the exact geometry of the corona, which is still largely uncertain. The AGN coronal emission is expected to be polarized, with the polarization percentage depending mainly on

the geometry and optical depth of the corona (Schnittman & Krolik 2010). X-ray polarimetry, in synergy with spectroscopic information, will help to remove the degeneracies between measured (cut-off energy and photon index) and physical (temperature and optical depth) parameters. This analysis will be possible through a single eXTP pointing, with broad-band spectroscopic observations in the soft (0.5–10 keV) and hard (2–30 keV) X-ray bands, together with polarimetric measurements in the 2–10 keV band. Due to the energy range of the LAD instrument, eXTP will largely focus on sources characterized by a low energy cut-off ($E_c \lesssim 150$ keV), which corresponds to coldest AGN coronae (e.g., Petrucci et al. 2001). We started to extensively investigate the nature of sources with the low energy cut-offs and temperatures using the best quality AGN broad-band spectra available with *NuSTAR*. We have selected a sample of AGN sources of nearly every known class (type-1 AGN, type-2 AGN, NLSy1s, non-blazar radiogalaxies), characterized by a low energy cut-off energy ($E_c \leq 150$ keV) as measured with the *Swift* Burst Alert Telescope (BAT) by Ricci et al. (2017). Our sample comprises ~ 40 AGN with available *NuSTAR* data. We fitted their spectra with detailed physical Comptonization models with two different coronal geometries (slab vs sphere), in order to investigate their properties, such as for instance where they lie in the $kT_e - \ell$ parameter space, where $\ell = L\sigma_T/Rm_ec^3$ is the compactness of the corona (e.g., Guilbert et al. 1983; Fabian et al. 2015). The statistical quality of the fit does not allow us to discriminate between different coronal geometries. Detailed SFA+LAD simulations show that with 100 ks exposure on a weak 1 mCrab AGN we will measure kT with an accuracy of about 40–50% for $kT < 150$ keV (see Fig. 3). While no statistically significant differences are found exploring two coronal geometries, the time-averaged polarization measurements with PFA will break this degeneracy. PFA observations will reach a MDP of about 2–3% in 100 ks exposure for an AGN with $\sim$ mCrab flux, providing fundamental information on the compact corona (Serafinelli et al. in preparation). Spectral-polarimetric analysis can be applied as well to investigate the physics and geometry of coronae in XRB (De Rosa et al. 2019).

2.4. Low Mass X-ray Binaries - LMXBs

Although the reflection component is found to be ubiquitous in XRBs containing BHs or NSs, a few NS LMXBs (such as the bright sources GX 5-1 and GX 9+9) do not show any evidence of this spectral feature. This is at odds with the fact that normally the reflection component (and in particular the Fe Kα line) is the strongest component in the soft spectral states, since in this case the disk should approach the compact object. The reasons for this lack can be manifold. It could be due to a strong ionization of the disk, which increases the amount of Compton broadening of the line making it hard to detect. Alternatively a combination of a high-inclination with respect to our line of sight together with a relatively small reflection amplitude and/or strong Comptonization of the line photons passing through the optically thick corona before reaching the observer, may produce a weak reflection component overwhelmed by the strong illuminating continuum. Spectral simulations of bright sources have shown that the large collecting area of eXTP can be useful for a detailed study of the reflection components in LMXBs, resulting in best-fit inner disk parameters with unprecedented precision. Moreover, it will also allow us to detect weak reflection components, if present. In particular, in the case of GX 9+9, a broadband (0.3–40 keV) spectrum acquired with BeppoSAX (50 ks exposure) and XMM-Newton (20 ks) did not show clear evidence of a reflection component, although a barely significant improvement was obtained with a reflection fraction of ~ 0.2 and a loose constraint on the inner disk radius of $R_{in} < 15$ R_g (Iaria et al. 2020). Using these parameters (R_{in}=15 R_g) we have simulated a 20-ks eXTP observation, obtaining clear residuals in the Fe K line energy range (see Fig. 4) if a reflection component is not included in the model. This would allow us to infer the inner disk radius with high precision (5–8%), which is important since in this kind of sources the disk probably

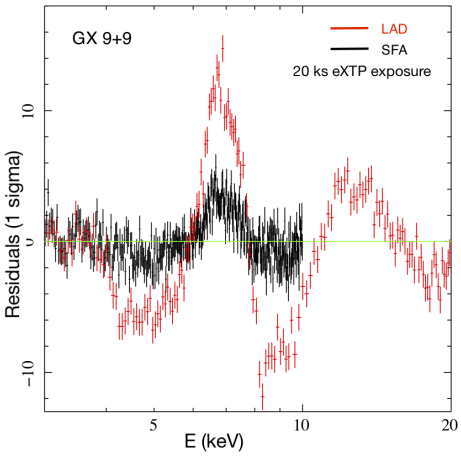

Fig. 4. Residuals with respect to the best-fit model of a 20 ks simulated eXTP data after removing the smeared reflection component. A broad emission line is evident in the Fe-K region, as well as other reflection features (such as the Fe edge and the Compton hump). Adapted from Iaria et al. (2020).

extends down to the NS surface or its boundary layer. We have demonstrated that 20 ks of eXTP/LAD observation would be able to reveal a weak reflection component with good statistics, giving therefore information on the inner disk parameters. eXTP data will allow us also to discriminate the origin of the soft seed-photons for the primary Comptonization component, whether they come from the NS boundary layer (with a spherical geometry) or from the inner disk (slab-like geometry).

3. NS Equation of State

The current loose theoretical constraints on the NS-EoS led to the emergence of several methods to indirectly probe it observationally, especially through measurements of mass and radius; no observation, however, has yet allowed us to measure both simultaneously with the required precision, $\sim 5\%$ (e.g Watts et al. 2019). In this section, we present new observational techniques to measure the compactness of NS and will describe the eXTP capability to put constraints on EoS families.

3.1. NS Radius-to-Mass ratio from accretion disk occultation

A new technique to measure the compactness of NSs will be made available by LAD data (La Placa et al. 2020). Provided that the inclination is high enough and the inner disk radius is small enough, the NS surface can occult part of the inner region of the disk by intercepting part of the photon trajectories starting behind the NS, with respect to the observer. Owing to the asymmetrical distribution of the redshift of the disk emission, the loss in flux imprinted by the occultation is not uniform over the Fe Kα line profiles, and thus distinguishable from a simple decrease in brightness. The impact of an occultation depends directly on the radius-to-mass ratio (R/M) of the NS, providing a new proxy for the NS size in X-ray spectroscopy. NSs with $R/R_g \gtrsim 6$ can all produce such spectral features in disks with $i \gtrsim 60°$, provided that the inner disk radius r_{in} extends close enough to their surface. The determination of such a small effect on current spectra is impractical, due to the insufficient signal-to-noise ratio. Introducing the `shaddisk` code into Xspec, dozens of eXTP/LAD simulations were produced with i ranging from 55° to 80° and R/R_g between 6 and 8, each with an exposure of 100 ks (La Placa et al. 2020). When the inner disk radius is at the surface of the star, R/R_g can be measured with better than 5% precision in all cases, and better than 3% in most. When $r_{in} = R + 1R_g$ it is only possible to place an upper limit on R/R_g: nevertheless, the latter constraint is always more stringent than the one put by the inner disk radius measurement alone. Moreover, the same precision as before is still attained in the cases in which both an upper and lower limit for R/R_g are found. Although the model was devised in the Schwarzschild metric, the results hold true for reasonably rotating NSs. Analysing with the same code the Fe Kα profile generated by rotating, oblate NSs, the value of their equatorial radius is retrieved within $\sim 5\%$ precision. Since this is the precision required to properly constrain the EoS, spectral analysis of occultation features adds to eXTP's already great potential in the study of NSs.

3.2. Optically thick coronae and accretion disk occultation

As the NS surface can cast a shadow on the inner accretion disk, which in high-inclination systems can affect the Fe line profile, in the same way an optically thick corona, as the one present in bright LMXBs and producing the primary Comptonization continuum, can occult part of the back side of the disk and produce similar distortions of the Fe line profile. This in turn may give important information on the size of the corona and the accretion disk–corona geometry. To test this hypothesis we have analysed (∼ 70 ks) XMM-Newton and (∼ 30 ks) NuSTAR spectra of the slow (P_{spin} ∼ 0.5) LMXB X-ray pulsar 4U 1822-37, with an inclination of i ∼ 80°–85°. Note that at such a high inclination the reflection component is really weak, since its strength decreases as $\cos i$. We have fitted the line profile with the `shaddisk` model described above, finding that current observations are insufficient to constrain the dimension of the compact corona. However, LAD+SFA simulations show that deformations of the relativistic iron line profile due to occultation by a corona extending up to 80 R_g (corresponding to the size of the pulsar magnetosphere and identified with the optically thick corona) will be clearly detected with a reasonable exposure of 150 ks (Gambino et al., MNRAS, submitted). For these exposures we find that the spectral distortions introduced by occultation will be detected at high statistical confidence, above 8 σ (see Fig. 5). In addition, we obtain an error box of about 14% of the corresponding measurement of the occultation radius of the optically thick (spherical) corona, with the precision of this measurement increasing for higher exposures. eXTP will allow us to apply this method in different systems to infer the size of the optically thick corona, the geometry of the accretion flow and the physical processes that intervene in the production of the observed emission.

The same technique of disk occultation from hot coronae could be in principle applied to accreting BHs such as XRBs and bright AGN (La Placa et al., in preparation).

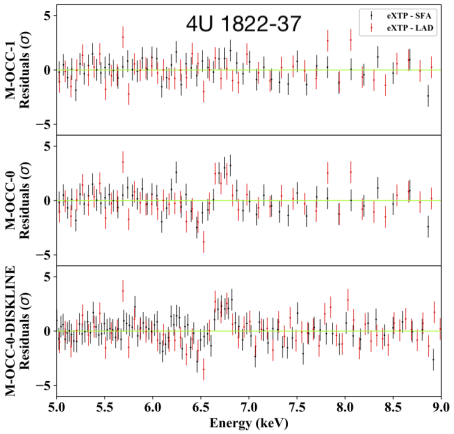

Fig. 5. Residuals of the simulated 150 ks eXTP spectra with respect to te models `shaddisk` including occultation (upper), `shaddisk` without occultation (middle) and a simple `diskline` (lower) assuming an optically thick, spherical corona with a radial size of 80 R_g.

3.3. Quasi-periodic oscillations

The fast quasi-periodic oscillations (QPOs) in the X-ray emission from NSs in low mass X-ray binaries can be used to constrain their equation of state. QPOs are believed to be produced in the inner regions of the accretion disk surrounding the compact object. Although their interpretation is still debated, in most models the QPO frequencies are interpreted as combinations of the fundamental frequencies of quasi-circular geodesics close to ISCO (Belloni & Stella 2014), i.e. the orbital frequency and the epicyclic frequencies. It has recently been shown (Maselli et al. 2020) that the fundamental frequencies of the geodesic motion around a NS can be computed as functions of the mass, angular momentum and quadrupolar momentum of the star, and thus can be exploited to constrain the NS equation of state. This approach has been used, as a proof of principle, to verify that one of the main geodesic models – the relativistic precession model (Vietri & Stella 1998; Stella & Vietri 1999) – is consistent with present observations of the QPOs from NSs. High precision QPOs measurements will be available with eXTP for a significant number of sources

(De Rosa et al. 2019). In addition to putting strong constraints on the EoS, the proposed model will provide key information on QPOs interpretation.

3.4. Mergers of compact stars in the two-families scenario

NSs can co-exist with stars made entirely of strange quark matter, called Strange Quark Stars (QSs, Drago et al. 2014). The existence of QSs is based on the validity of the Bodmer-Witten hypothesis, stating that lumps of strange quark matter are more stable than iron: QSs are stable even in the absence of gravity. The co-existence of NSs and QSs allows for the existence of compact stellar objects with very small radii (∼11 km or less) and not too large masses ($\lesssim$ 1.5–1.6 $M_\odot$) and, at the same time, allows the existence of very massive objects, with masses up to 2.5–2.6 $M_\odot$ and not too small radii. The first class of objects would correspond to NSs made of neutrons, protons, hadronic resonances and hyperons (the production of these particles makes the EoS soft and explains the small radii), while the second class of objects would be that of QSs. The two-families scenario has many testable implications. The most obvious one is the ability to explain the existence of stars with R $\lesssim$ 11.5 km and M $\sim$ 1.4–1.5 $M_\odot$, which is not possible unless a strong first order phase transition is present in the compact stars. This prediction can be tested by eXTP. Core science of the mission will be in fact devoted to observation of rotation-powered pulsars that will allow us to measure NS mass and radius in about 10 sources at the few percent level (considering the anticipated Observing Plan, Watts et al. 2019). Other predictions are associated with mergers. Three types of mergers are possible in the two-families scenario: NS–NS, NS–QS and QS–QS (e.g. Drago & Pagliara 2018; De Pietri et al. 2019), and, assuming this scenario, the merger associated with GW170817 can only be explained as a NS–QS merger. This is because a NS–NS merger with a total mass of about 2.73 $M_\odot$ would lead to a direct collapse to a BH (the maximum mass of a non-rotating NS is only about 1.5–1.6 $M_\odot$ in that scenario and the threshold mass is about 2.5 $M_\odot$) while the total mass of GW170817 is most likely too small to be a QS–QS merger. This wider range of possibilities, with respect to the one-family scenario, allows an average tidal deformability $\tilde{\Lambda} \gtrsim 400$ while having $R_{1.5} \lesssim 12$ km for M=1.5 $M_\odot$ star for a NS–QS merger, which is not possible in the one-family case (Burgio et al. 2018). The main predictions of the two-families scenario concerning mergers are:
(a) direct collapse to a BH for total masses $\gtrsim 2.5 M_\odot$, in the case of a NS–NS merger. This is the most striking prediction of the model since a direct collapse is impossible in all other scenarios if the total mass is smaller than that of GW170817. In that merger a direct collapse has been ruled out, which is possible within the two-families if GW170817 is a NS–QS merger (Drago & Pagliara 2018);
(b) the kilonova signal for a NS–BH merger is strongly suppressed with respect to the one-family case, due to the small NS radii. This prediction should be testable with the Vera Rubin Observatory (Di Clemente et al. 2021);
(c) the formation of deconfined quark matter does not lead to a softening of the Equation of State in the two-families scenario, at variance with what is predicted in all the other scenarios in which quark matter forms. This implies that the formation of quark matter is *not* associated with an increase of the frequency of the GW signal (it could even lead to a decrease of the frequency De Pietri et al. 2019). If the post-merger GW emission is observed this prediction can be tested since the two-families scenario predicts the formation of a QS in the post-merger in all cases in which there is not a direct collapse to a BH.
The unique eXTP combination of field of view, large effective area, broad energy band, spectral resolution and polarization capabilities, will allow us to address fundamental questions related to mergers events by observing the EM counterpart of GW events (in't Zand et al. 2019, and references therein). The WFM will be able to confirm or exclude different prompt Gamma Ray Burst (GRB) emission models detecting EM signals from the remnant on a relevant time scale (from ∼ 1 s to longer).

4. Scientific simulations: response matrices and background

In March 2021 a new version of the eXTP matrices has been released at the mission webpage `https://www.isdc.unige.ch/extp/`. The simulation package included the goal and requirement configurations that will be discussed in a more detailed below.

LAD. We provided matrices referring to End-of-Life conditions. Earlier in the mission lifetime, the spectral resolution (which depends on operational temperature) will be not yet degraded by radiation damage. Goal matrices refer to the baseline effective area increased by a factor of $\sim$ 7% obtained with a collimator opening area ratio of 0.75. We also released matrices referring to the selection of only single-anode events (offering the higher spectral resolution of FWHM=200 eV at 6 keV), with a reduced effective area to 40% of the baseline at 6 keV. The LAD background was determined using an updated mass model with the eXTP spacecraft design (from the model as provided in March 2020) in Geant-4 simulator. 40 LAD modules were considered with a realistic placement on optical bench, and updated module design (materials, spacing between layers, etc). Through Monte Carlo simulator (Campana et al. 2013) we included the contributions to the overall LAD background in an equatorial low-Earth orbit (outside SAA). The LAD background in the baseline configuration is 600 cts/s in 2–30 keV.

WFM: In order to allow scientists to obtain a sense of the WFM coverage, together with arf, rmf and bkg files, a 1-year integrated exposure map of the WFM was also provided. The exposure is added if a position is covered by at least 10 cm^2 per camera. The WFM background has been compiled from calculations of the particle-induced background (through Geant-4) and the diffuse cosmic X-ray background (CXB) (Campana et al. 2012) and amounts to 590 cts/s/camera-pair in the whole energy band. The contribution from other point sources in the field of view varies over the sky, from a negligible contribution close to the Galactic poles, up to 2500 cts/s/camera-pair close to Sco X-1, with an average over the whole sky of $\sim$ 240 counts/s/camera-pair. Thus, the sensitivity can be up to a factor of 2 worse than that based on the provided background.

SFA: For the 9 SFA payload two kinds of configurations have been considered: a multilayer (Au+10 nm of carbon composite) coated Wolter-I mirror and a gold coating, producing two different effective areas around 2 keV. A study of possible configuration and performance is presented in Qi et al. 2020. As for the LAD, the SFA background is obtained through the Monte Carlo simulation based on the mass model of the platform and payload through Geant-4. The total SFA background includes the particle background with a constant rate of 0.003 cts/s/cm^2/keV and the aperture CXB.

PFA: As for the SFA, the 4 PFA mirrors have the baseline configuration of gold coating, while the mixed coating is considered as an optimized scheme (Qi et al. 2020). The total PFA background comprises particle background and the CXB. The particle background spectrum is modeled with a power-law returning an average rate of 0.0033 cts/sec/cm^2/keV in 2–8 keV energy range. Large part of the high energy community has been involved in scientific simulations that have been used to optimize the mission and instrument performances and to define the scientific requirements (described in Scientific Requirement, Mission requirement and Observing plan documents.

5. Conclusions

Detailed scientific simulations demonstrate the unprecedented progress that eXTP will make in the study of matter accreting under SFG regimes and in the EoS determination through mass and radius measurements. eXTP will address many fundamental issues in BH and NS astrophysics, such as the physics and geometry of the hot coronae. The eXTP effective area, which will greatly improve the photon counting statistics, will make available the use of new and more accurate analysis (e.g. disk occultation) to constrain accretion properties and geometry nearby compact objects. Moreover, the combined spectral-polarimetric and spectral-timing information

will allow us to measure the same physical quantity using different techniques: eXTP observations will significantly reduce the systematic uncertainties linked to modeling. The presented activities also included support for scientific simulations to the whole community such as the release of response matrices and background files, and studies of the mission scientific requirements.

Affiliations

[11] Dipartimento di Fisica, Universitá degli Studi di Cagliari, SP Monserrato-Sestu, KM 0.7, 09042, Monserrato, Italy

[12] INAF - Osservatorio di Astrofisica e Scienza dello Spazio di Bologna, Via Gobetti 93/3, 40129 Bologna, Italy

[13] INAF - Istituto di Astrofisica Spaziale e Fisica Cosmica Palermo, via Ugo La Malfa 153, I-90146 Palermo, Italy

[14] INAF - Istituto di Radioastronomia, Via Gobetti 101, I-40129 Bologna, Italy

[15] INAF - Osservatorio Astronomico di Capodimonte, Salita Moiariello 16, I-80131 Napoli, Italy

[16] INAF - Osservatorio Astrofisico di Arcetri, Largo Enrico Fermi 5, 50125, Firenze, Italy

[17] Dipartimento di Fisica e Astronomia, Università di Padova, Via F. Marzolo 8, I-35131 Padova, Italy

[18] INAF - Osservatorio Astronomico di Brera, Via Emilio Bianchi 46, 23807, Merate, LC, Italy

Acknowledgements. We acknowledge financial contribution from the agreement ASI-INAF n.2017-14-H.O

References

Belloni, T. M. & Stella, L. 2014, Space Sci. Rev., 183, 43

Burgio, G. F., Drago, A., Pagliara, G., Schulze, H. J., & Wei, J. B. 2018, ApJ, 860, 139

Campana, R., Feroci, M., Del Monte, E., et al. 2012, in Society of Photo-Optical Instrumentation Engineers (SPIE) Conference Series, Vol. 8443, Space Telescopes and Instrumentation 2012: Ultraviolet to Gamma Ray, ed. T. Takahashi, S. S. Murray, & J.-W. A. den Herder, 84435O

Campana, R., Feroci, M., Del Monte, E., et al. 2013, Experimental Astronomy, 36, 451

Connors, P. A. & Stark, R. F. 1977, Nature, 269, 128

Dauser, T., Wilms, J., Reynolds, C. S., & Brenneman, L. W. 2010, MNRAS, 409, 1534

De Pietri, R., Drago, A., Feo, A., et al. 2019, ApJ, 881, 122

De Rosa, A., Uttley, P., Gou, L., et al. 2019, Science China Physics, Mechanics, and Astronomy, 62, 29504

Di Clemente, F., Drago, A., & Pagliara, G. 2021, arXiv e-prints, arXiv:2106.16151

Drago, A., Lavagno, A., & Pagliara, G. 2014, Phys. Rev. D, 89, 043014

Drago, A. & Pagliara, G. 2018, ApJ, 852, L32

Fabian, A. C., Lohfink, A., Kara, E., et al. 2015, MNRAS, 451, 4375

Fabian, A. C., Rees, M. J., Stella, L., & White, N. E. 1989, MNRAS, 238, 729

Falanga, M., Bakala, P., La Placa, R., et al. 2021, MNRAS, 504, 3424

Guilbert, P. W., Fabian, A. C., & Rees, M. J. 1983, MNRAS, 205, 593

Haardt, F. & Maraschi, L. 1991, ApJ, 380, L51

Iaria, R., Mazzola, S. M., Di Salvo, T., et al. 2020, A&A, 635, A209

in't Zand, J. J. M., Bozzo, E., Qu, J., et al. 2019, Science China Physics, Mechanics, and Astronomy, 62, 29506

La Placa, R., Stella, L., Papitto, A., et al. 2020, ApJ, 893, 129

Maselli, A., Pappas, G., Pani, P., et al. 2020, Astrophys. J., 899, 139

Petrucci, P. O., Haardt, F., Maraschi, L., et al. 2001, ApJ, 556, 716

Qi, L. Q., Li, G., Xu, Y. P., et al. 2020, Nuclear Instruments and Methods in Physics Research A, 963, 163702

Ricci, C., Trakhtenbrot, B., Koss, M. J., et al. 2017, ApJS, 233, 17

Santangelo, A., Zane, S., Feng, H., et al. 2019, Science China Physics, Mechanics, and Astronomy, 62, 29505

Schnittman, J. D. & Krolik, J. H. 2009, ApJ, 701, 1175
Schnittman, J. D. & Krolik, J. H. 2010, ApJ, 712, 908
Stark, R. F. & Connors, P. A. 1977, Nature, 266, 429
Stella, L. & Vietri, M. 1999, Phys. Rev. Lett., 82, 17
Taverna, R., Marra, L., Bianchi, S., et al. 2021, MNRAS, 501, 3393
Taverna, R., Zhang, W., Dovčiak, M., et al. 2020, MNRAS, 493, 4960
Vietri, M. & Stella, L. 1998, Astrophys. J. Lett., 507, L45
Watts, A. L., Yu, W., Poutanen, J., et al. 2019, Science China Physics, Mechanics, and Astronomy, 62, 29503
Weisskopf, M. C., Ramsey, B., O'Dell, S., et al. 2016, in Society of Photo-Optical Instrumentation Engineers (SPIE) Conference Series, Vol. 9905, Space Telescopes and Instrumentation 2016: Ultraviolet to Gamma Ray, ed. J.-W. A. den Herder, T. Takahashi, & M. Bautz, 990517
Zhang, S., Santangelo, A., Feroci, M., et al. 2019, Science China Physics, Mechanics, and Astronomy, 62, 29502